

BKT transitions of the XY and six-state clock models on the various two-dimensional lattices

Yutaka Okabe and Hiromi Otsuka

Department of Physics, Tokyo Metropolitan University, Hachioji, Tokyo 192-0397, Japan

E-mail: okabe@phys.se.tmu.ac.jp

14 January 2025

Abstract. In a two-dimensional (2D) spin system, the XY model, characterized by planar rotational symmetry, exhibits a unique phenomenon known as the Berezinskii-Kosterlitz-Thouless (BKT) transition. In contrast, the clock model, which introduces discrete rotational symmetry, exhibits the BKT transition at two different temperatures due to this discreteness. In this study, we numerically investigate the BKT transition for XY and six-state clock models over various two-dimensional lattices. We employ two primary methods: the Monte Carlo method, which analyzes the size dependence of the ratio of the correlation functions for two different distances, and a machine-learning approach to classify the different phases — namely, the low-temperature ordered phase, the intermediate BKT phase, and the high-temperature disordered phase. We identify the BKT transition temperatures for the XY and six-state models on honeycomb, kagome, and diced lattices. Combined with the previously calculated data for the triangular lattice, we then compare these values with the second-order phase transition temperatures of the 2D Ising model, for which exact solutions are known. Our results indicate that the ratio of the BKT transition temperatures for each lattice relative to the Ising model transition temperatures are close, although the values are not universal.

Keywords: BKT transition, XY model, clock model, Ising model, Monte Carlo simulation, machine-learning study

1. Introduction

Two-dimensional (2D) spin systems with continuous XY symmetry undergo a unique phase transition known as the Berezinskii-Kosterlitz-Thouless (BKT) transition [1, 2, 3, 4]. In the BKT phase, which exhibits quasi-long-range order, the correlation function decays according to a power law. The q -state clock model, a discrete counterpart of the XY model, experiences two BKT transitions when $q > 4$ due to its discrete nature [5, 6].

However, the numerical analysis of the BKT transition is challenging. The correlation length diverges more rapidly than any power law during the BKT transition, and there are logarithmic corrections [7] that complicate matters. These characteristics make it difficult to accurately determine the BKT transition point through finite-size calculations. Monte Carlo simulation is a widely used method for the numerical analysis of many particle systems [8]. The finite-size scaling (FSS) study [9, 10] of the Binder ratio [11], which is essentially a moment ratio, serves as a powerful tool for studying second-order phase transitions. However, the Binder ratio is less effective for analyzing the BKT transition [12] due to the presence of multiplicative logarithmic corrections [4, 7]. Other quantities also exhibit FSS behavior with a single variable, similar to the Binder ratio. Some of these quantities are less sensitive to logarithmic corrections than the Binder ratio. For instance, the ratio of correlation functions at different distances [13] exhibits this property. In addition, the size-dependent second-moment correlation length for a finite system, denoted as $\xi(L)$, has often been applied to spin glass problems [14]; the FSS of $\xi(L)/L$ retains the same form with a single scaling variable. Surungan *et al.* [15] made the Monte Carlo study of the correlation ratio and the size-dependent second-moment correlation length for the q -state clock model. They observed the collapsing curves of different sizes at intermediate temperatures and the spray out at lower and higher temperatures, which demonstrates two BKT transitions.

In addition to conventional approaches, new numerical strategies are developing. Recent advances in machine-learning-based techniques have been applied to fundamental research, such as statistical physics [16]. Carrasquilla and Melko [17] used a technique of supervised learning for image classification, which is complementary to the conventional approach of studying interacting spin systems. They classified and identified a high-temperature paramagnetic phase and a low-temperature ferromagnetic phase of the 2D Ising model by using data sets of spin configurations. Shiina *et al.* [18] extended and generalized this machine-learning approach to studying various spin models including the multi-component systems and the systems with a vector order parameter. The configuration of a long-range spatial correlation was treated instead of the spin configuration itself. Not only the second-order and the first-order transitions but also the BKT transition was studied. They detected two BKT transitions for the six-state clock model. Tomita *et al.* [19] made further progress in the machine-learning study of phase classification. When the cluster update is possible in the Monte Carlo simulation, the Fortuin-Kasteleyn (FK) [20, 21] representation-based improved estimators [22, 23] for the configuration of two-spin correlation were employed as an alternative to the

ordinary spin configuration. This method of improved estimators was applied not only to the classical spin models but also the quantum Monte Carlo simulation.

In the study of lattices, most investigations of the BKT transition have focused on the square lattice. Highly accurate data on the BKT transition temperature are available for the XY model, as reported by Hasenbusch [24], and for the q -state clock model, as provided by Tomita and Okabe [25]. More recently, tensor network methods have been applied to the study of the XY model [26] and the q -state clock model [27]. The list of the numerical estimates of the BKT temperature of the XY model has been tabulated in Table II of Ref. [26], and those of the q -state clock model in Table S1 of the Supplemental Material of Ref. [27]. An exception is the study by Sorokin [28] for the XY model on a triangular lattice. In addition, the ferromagnetic XY model on a triangular lattice, along with the six-state clock model, was numerically analyzed in the context of the antiferromagnetic Ising model with next-nearest neighbor interactions on a triangular lattice, relating these findings to the six-state clock universality [29]. Recently, two research groups [30, 31] have studied the BKT transition of the XY model on a honeycomb lattice, motivated by its relevance to the solution of the n -vector loop model [32, 33].

In this paper, we perform a systematic study of the BKT transition for both the XY and six-state clock models over various two-dimensional lattices. Our calculations include the honeycomb lattice, the kagome lattice, and the diced lattice. For the triangular lattice, we refer to the results discussed in the appendices of a previous study [29]. Exact solutions are known for Ising models on several 2D lattices [34, 35, 36, 37]. We discuss the relationship between the BKT transition temperatures of the XY and the six-state clock models and the second-order phase transition temperature of the Ising model on various lattices.

The rest of the paper is organized as follows: In Sec. 2, we explain the models and simulation methods. Section 3 is devoted to the results of the Monte Carlo study and the machine-learning study. The comparison of the BKT temperatures and the second-order phase transition temperatures of the 2D Ising model is discussed in Sec. 4. The summary and discussion are given in Sec. 5.

2. Models and simulation methods

2.1. Model

A q -state clock model is defined by the following Hamiltonian:

$$H = -J \sum_{\langle ij \rangle} \vec{s}_i \cdot \vec{s}_j = -J \sum_{\langle ij \rangle} \cos(\theta_i - \theta_j), \quad (1)$$

where the spins \vec{s}_i located on lattice sites are planar spins restricted to align at q discrete angles ($\theta = 2n\pi/q$ with $n = 1, \dots, q$). In the limit as q approaches infinity, this model becomes an XY model. The summation is over the nearest-neighbor sites of 2D lattices. We examine the triangular, honeycomb, kagome, and diced lattices, which are illustrated

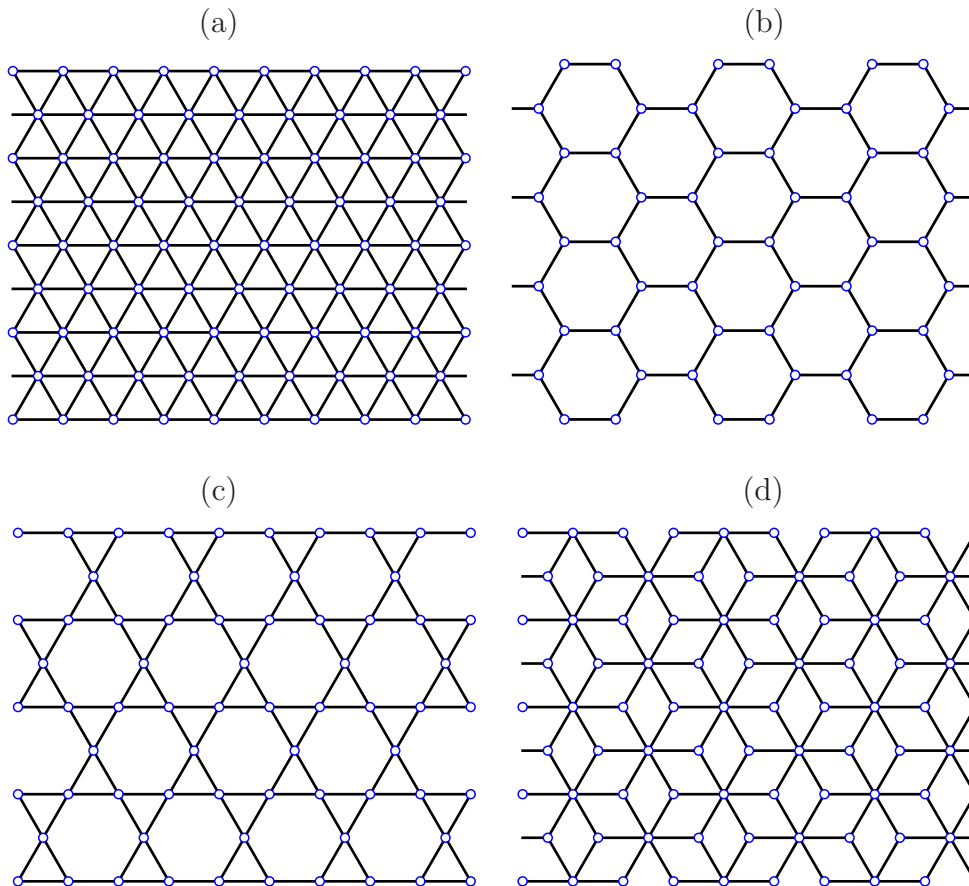


Figure 1. The illustration of (a) triangular, (b) honeycomb, (c) kagome, (d) diced lattices.

in Fig. 1. The system sizes considered are $\frac{3}{2}L \times L$, with periodic boundary conditions imposed for the numerical simulations.

2.2. Monte Carlo Study

We utilize two approaches to study the BKT transitions. First, we conduct Monte Carlo simulations. In this process, we implement the multi-cluster spin-flip Swendsen-Wang algorithm [38] and incorporate the embedded scheme of Wolff [39] for constructing clusters of clock spins to overcome the problem of the long autocorrelation time near the critical temperature. Additionally, we combine the replica exchange method of parallel tempering [40].

We calculate the ratio of the correlation functions of different distances, $R(T) = \langle g(L/2) \rangle / \langle g(L/4) \rangle$; for the two distances, we chose $L/2$ and $L/4$. The correlation function with the distance r is given by

$$g_i(r) = \vec{s}_i \cdot \vec{s}_{i+r} = \cos(\theta_i - \theta_{i+r}). \quad (2)$$

The correlation ratio has a single scaling variable for FSS

$$R(T) = \frac{\langle g(L/2) \rangle}{\langle g(L/4) \rangle} = \tilde{f}(L/\xi), \quad (3)$$

as in the Binder ratio [11]. Here, ξ stands for the correlation length. At the critical region, where the correlation length ξ is infinite, the correlation ratio does not depend on the system size L . Thus, we expect the data collapsing of different sizes in the BKT phase. Above the upper BKT temperature T_2 and below the lower BKT temperature T_1 , the data of different sizes begin to separate. In the case of the BKT transition, the correlation length diverges as

$$\xi \propto \exp(c/\sqrt{|t|}), \quad (4)$$

where $t = T - T_{1,2}$.

2.3. Machine-Learning Study

The second approach is the machine-learning study, developed by Shiina *et al.* [18], to classify the ordered, the BKT, and the disordered phases for the clock models. This work extends and generalizes the research conducted by Carrasquilla and Melko [17], who focused on the Ising model. The configuration of a long-range spatial correlation with the distance of $L/2$ is treated rather than the spin configuration itself. In this way, a similar treatment has been given to various spin models, including multi-component systems and systems with a vector order parameter. The study examines not only the second-order and first-order transitions but also the BKT transition. For the training data, we collected typical configurations from each phase, the ordered, the BKT, or the disordered, and the test data were evaluated across all temperatures. We implemented a fully connected neural network using a standard library of TensorFlow of the 100-hidden unit model. A cross-entropy cost function, supplemented with an L2 regularization term, was employed. The neural networks were trained using the Adam optimization method [41].

3. Results

3.1. Results of Monte Carlo Study

3.1.1. XY model The Monte Carlo results of the XY model on the honeycomb, kagome, and diced lattices are presented in Fig. 2. The correlation ratio, $R(T)$, is plotted in the left panels of Fig. 2. The system sizes are $L = 48, 72, 96, 144, \text{ and } 192$.

The collapse of the curves representing different system sizes in the plot of the correlation ratio, $R(T)$, is indicative of the BKT phase. The observed phenomenon is a direct consequence of the power law behavior exhibited by the correlation function in the BKT phase. We conduct a FSS analysis. In the inset of Fig. 2, we present the FSS plots based on the exponential divergence of the correlation length, as expressed by Eq. (4), where $X(c, T) = L/\exp(c/(|T - T_{\text{BKT}}|))$, The rough estimate of the BKT

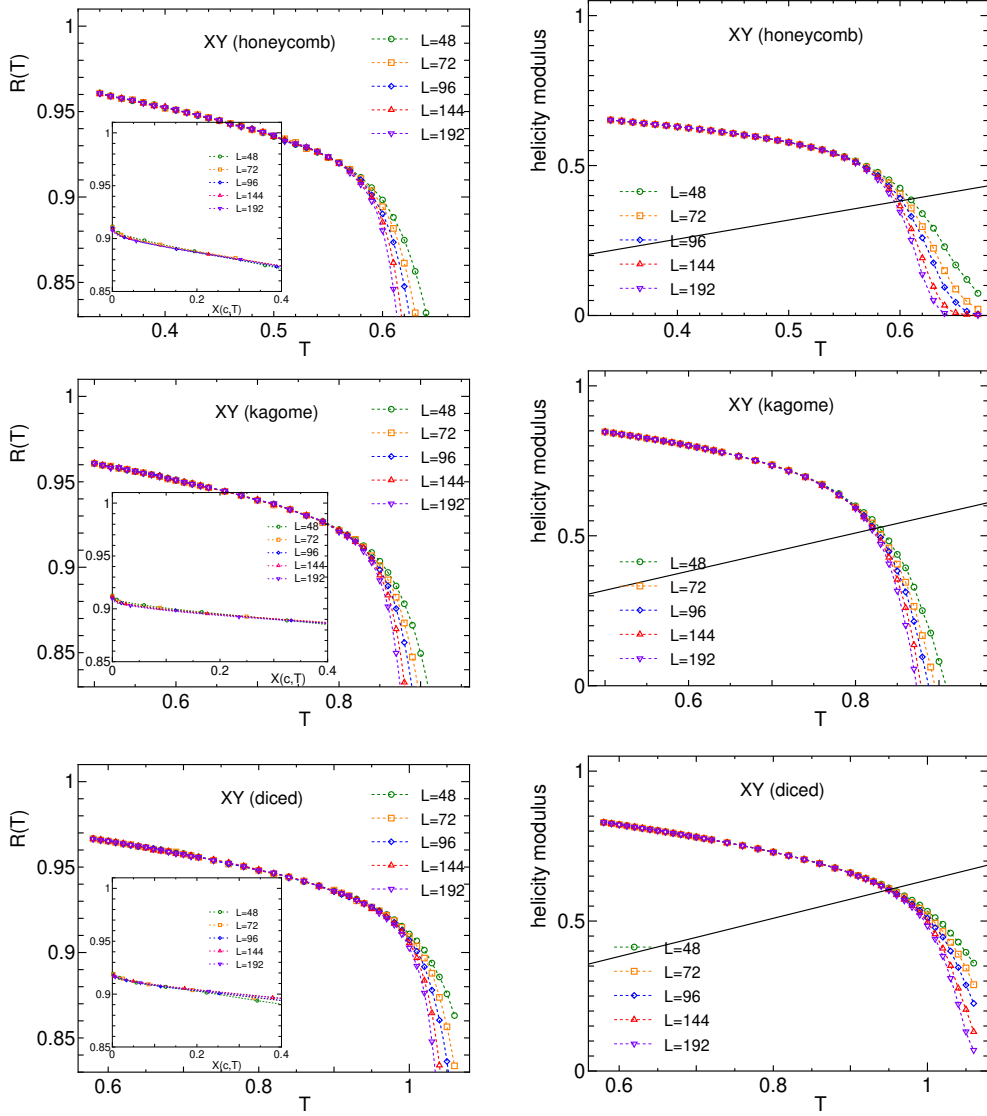


Figure 2. (left panel) The plot of the correlation ratio $R(T)$ of the XY model for the honeycomb, kagome, and diced lattice. The system sizes are 48, 72, 96, 144, and 192. In the inset, the FSS plots are given, where $X(c, T) = L / \exp(c_{\text{BKT}} / (\sqrt{|T - T_{\text{BKT}}|}))$. (right panel) Helicity modulus for each lattice. We give the straight line $(2/\pi)T$.

temperature for the honeycomb lattice is $T_{\text{BKT}} = 0.573$. A rough estimates of the BKT temperature for the kagome and diced lattices are 0.825 and 0.965, respectively. These estimates of the BKT temperatures on the honeycomb, kagome and diced lattices are presented in Table 1.

The helicity modulus, Υ , obtained by a measure of the resistance to an infinitesimal spin twist across the system along one coordinate, is an efficient method to calculate the BKT phase-transition temperature [45]. Following the derivation process of Ref. [46, 47],

Table 1. The list of BKT temperatures of the XY model and the six-state clock model together with the exact solutions of the Ising model. The second column lists the coordination numbers for each lattice. The exact second-order transition temperatures are provided in the third column, along with their values divided by the coordination number in the parentheses. The numerical estimates for the BKT transition of the XY model, as well as the two BKT transitions of the six-state clock model, are presented in the fourth, fifth, and sixth columns. Additionally, the normalized values, divided by the exact T_c values of the Ising model, are included in the parentheses.

	n.n.	T_c^{Ising} (/n.n.)	T_{BKT} (/ T_c^{Ising})	T_1 (/ T_c^{Ising})	T_2 (/ T_c^{Ising})
square [24, 25]	4	2.2692 (0.567)	0.8929 (0.394)	0.7014 (0.309)	0.9008 (0.397)
triangular [29]	6	3.6410 (0.607)	1.43 (0.393)	1.12 (0.308)	1.44 (0.395)
honeycomb [44]	3	1.5186 (0.506)	0.573 (0.377)	0.455 (0.300)	0.579 (0.381)
kagome [44]	4	2.1433 (0.536)	0.825 (0.385)	0.645 (0.301)	0.835 (0.390)
diced [44]	4 (3,6)	2.4055 (0.601)	0.965 (0.401)	0.755 (0.314)	0.975 (0.405)

the expression of helicity modulus can be written as

$$\Upsilon = \frac{1}{L^2} \left[\left\langle \sum_{\langle i,j \rangle} \cos(\theta_i - \theta_j) (\hat{x} \cdot \hat{\epsilon}_{ij})^2 \right\rangle - \frac{1}{T} \left\langle \left(\sum_{\langle i,j \rangle} \sin(\theta_i - \theta_j) (\hat{x} \cdot \hat{\epsilon}_{ij}) \right)^2 \right\rangle \right]. \quad (5)$$

In this context, $\hat{\epsilon}_{ij}$ represents a unite vector pointing from site j to site i . The symbol \hat{x} is used to denote a selected basis vector in one coordinate. As postulated by the renormalization-group theory [3], a universal relation exists between the helicity modulus and the BKT transition temperature. The BKT transition is distinguished by a discontinuity in the helicity modulus, which undergoes a transition from a value of $2T/\pi$ (in units of the Boltzmann constant $k_B = 1$) to zero at the critical temperature. This critical temperature, denoted as T_{BKT} , can be estimated by identifying the point of intersection between the helicity modulus $\Upsilon(T)$ and a straight line with the equation $\Upsilon = 2T/\pi$.

We calculate the helicity modulus, and the results for the honeycomb, kagome and diced lattices are plotted in the right panel of Fig. 2. In the plot of the helicity modulus, we give the straight line $(2/\pi)T$. The point of intersection gives a universal jump. The observed intersection yields a temperature that corresponds to the BKT temperature determined by the FSS of the correlation ratio. A systematic analysis of finite size effects has been carried out [48, 49].

3.1.2. six-state clock model The Monte Carlo results for the correlation ratio, $R(T)$, of the six-state clock model on the honeycomb, kagome, and diced lattices are presented in the left panel of Fig. 3. The system sizes are 48, 72, 96, 144, and 192. It can be observed that the curves for different sizes collapse at intermediate temperature regimes and the spray out at lower and higher temperatures, while the lower and higher temperatures, a spray-out effect is evident. The divergence of the curves at lower and higher temperatures indicates the occurrence of BKT transitions. In the inset, we present the FSS plots based on the exponential divergence of the correlation length, where $X(c, T) = L / \exp(c_{1,2}/(|T - T_{1,2}|))$. The BKT temperatures are estimated to be approximately $T_2 = 0.579$ and $T_1 = 0.455$ for the honeycomb lattice. For the kagome and diced lattices, the rough estimates are as follows: $T_2 = 0.835$, $T_1 = 0.645$ and $T_2 = 0.975$, $T_1 = 0.755$, respectively.

The helicity modulus for the clock model was calculated and the results are plotted in the right panel of Fig. 3. In the plot of helicity modulus, we provide the straight line $(2/\pi)T$. The crossing point gives a universal jump. The q -state clock model, which is a discrete version of the XY model, experiences two BKT transitions because of the discreteness. We observe that there is no anomaly in helicity modulus for the lower transition, T_1 .

The behavior of the BKT transition of the high-temperature BKT of the six-state clock model is analogous to that observed in the XY model. The BKT temperature of the XY model for the honeycomb lattice is approximately $T_{\text{BKT}} = 0.573$, which is slightly lower than $T_2 = 0.579$ of the six-state clock model. This is similar to the square lattice case as well as the triangular lattice case, as shown by the previous studies [25, 29]. This behavior is also observed for the kagome and diced lattices.

The rough estimates of T_1 and T_2 of the six-state clock model on the honeycomb, kagome and diced lattices are also tabulated in Table 1.

3.2. Results of Machine-Learning Study

The following subsection presents the findings of the machine-learning investigation. The output layers averaged over a test set as a function of T for the six-state model on the honeycomb, kagome, and diced lattices are illustrated in Fig. 4. The system sizes are 24, 48, and 72. For the honeycomb lattice, the samples of T in the ranges of $0.32 \leq T \leq 0.41$, $0.46 \leq T \leq 0.55$ and $0.62 \leq T \leq 0.71$ are used for training data, for the low-temperature, middle-temperature, and high-temperature training data, respectively. The predicted probabilities of the phases are illustrated as a function of temperature. It is evident that three distinct phases can be discerned: the ordered phase, the BKT phase, and the disordered phase. The size-dependent $T_{1,2}(L)$ is estimated from the point at which the probabilities of predicting two phases are equal to 50%. The approximate values of T_1 and T_2 are 0.43 and 0.60, respectively. The estimates are in accordance with those derived from the Monte Carlo study. However, the BKT phase is slightly broader, which is consistent with the findings reported for the square lattice [18]. This is

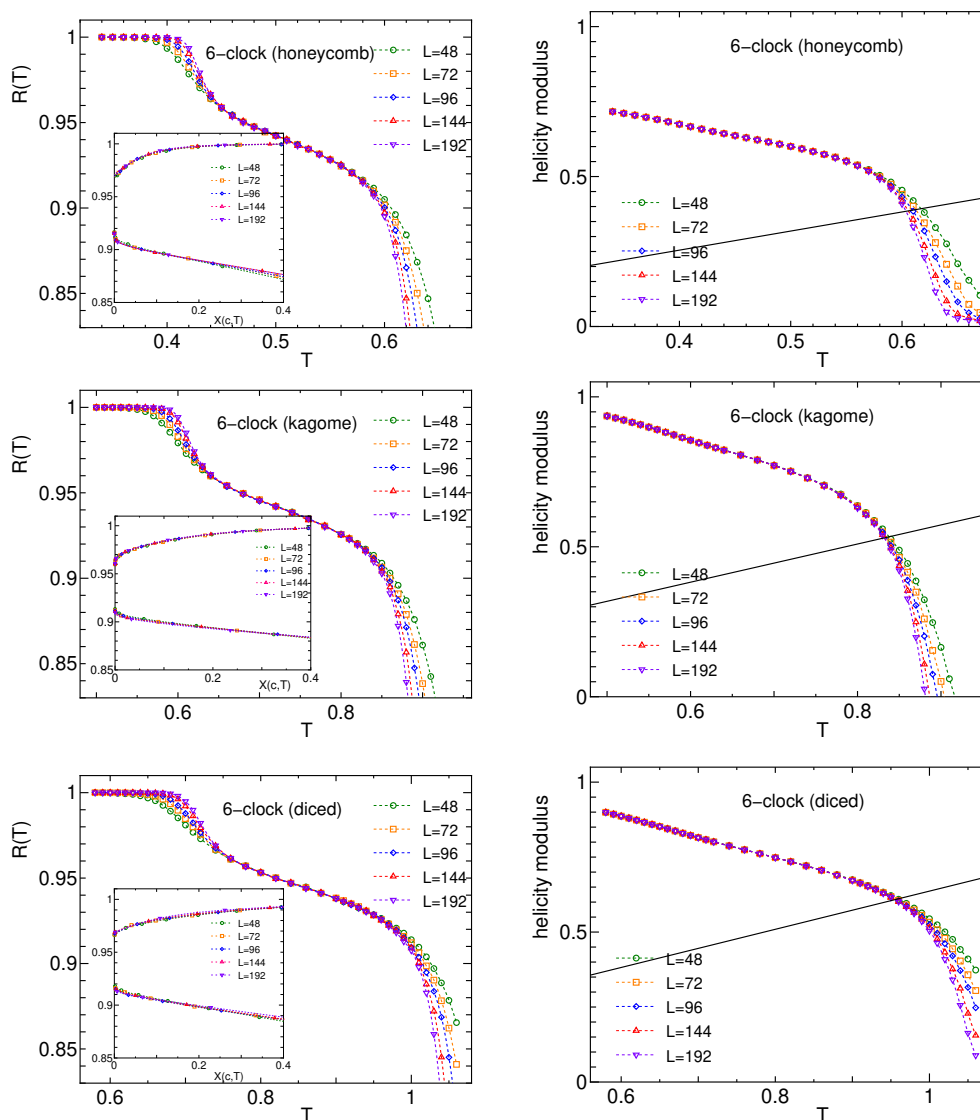


Figure 3. (left panel) The plot of the correlation ratio $R(T)$ of the six-state clock model for the honeycomb, kagome, and diced lattice. The system sizes are 48, 72, 96, 144, and 192. In the inset, the FSS plots are given, where $X(c, T) = L / \exp(c_{1,2} / (\sqrt{|T - T_{1,2}|}))$. (right panel) Helicity modulus for each lattice. We give the straight line $(2/\pi)T$.

a consequence of the finite size effect. The size used by the machine learning method is smaller than that of the Monte Carlo method. Additionally, the logarithmic correction might be less significant for the Monte Carlo method, which deals with correlation ratios.

For the kagome lattice, the samples of T in the ranges $0.51 \leq T \leq 0.60$, $0.69 \leq T \leq 0.78$ and $0.88 \leq T \leq 0.97$ are employed as training data. In accordance with the methodology previously employed for the honeycomb lattice, the rough estimates of T_1 and T_2 are 0.63 and 0.85, respectively. These estimates are once again found to be compatible with those obtained from the Monte Carlo study. In the case of the diced

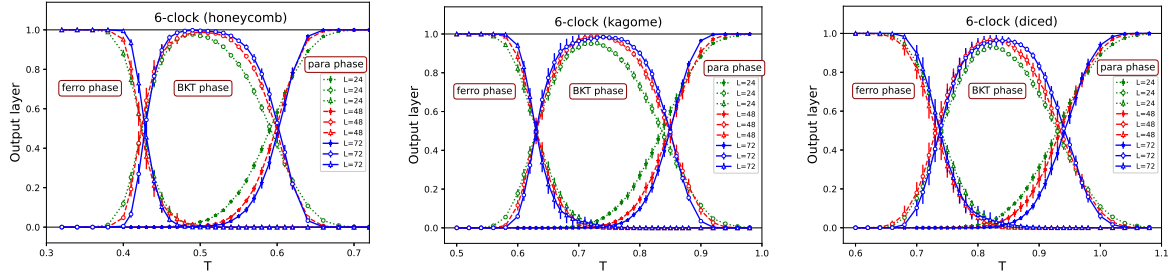


Figure 4. The machine-learning study of the six-state clock models on the honeycomb, kagome, and diced lattices. The output layer averaged over a test set as a function of T are plotted. The system sizes are $L = 24, 48,$ and 72 . For the honeycomb lattice, the samples of T in the ranges $0.32 \leq T \leq 0.41$, $0.46 \leq T \leq 0.55$ and $0.62 \leq T \leq 0.71$ are used for training data. For the kagome lattice, the samples of T in the ranges $0.51 \leq T \leq 0.60$, $0.69 \leq T \leq 0.78$ and $0.88 \leq T \leq 0.97$ are used for training data. For the diced lattice, the samples of T in the ranges $0.61 \leq T \leq 0.70$, $0.79 \leq T \leq 0.88$ and $0.98 \leq T \leq 1.07$ are used for training data.

lattice, the training data set is comprised of samples of T in the ranges $0.61 \leq T \leq 0.70$, $0.79 \leq T \leq 0.88$ and $0.98 \leq T \leq 1.07$. The approximate values of T_1 and T_2 are 0.74 and 0.94, respectively.

4. Comparison of BKT temperatures

Exact solutions of the Ising models on various 2D lattices have been obtained. The square-lattice Ising model was exactly solved by Onsager [34]. The exact solutions for the transition temperatures have also been obtained for the triangular and honeycomb lattices [35], and for the kagome and diced lattices [36, 37]. The critical temperatures of the second-order transition for these lattices are

$$\begin{aligned}
 T_c^{\text{square}} &= \frac{2}{\ln(1 + \sqrt{2})} = 2.26919 \dots \\
 T_c^{\text{triangular}} &= \frac{4}{\ln 3} = 3.640964 \dots \\
 T_c^{\text{honeycomb}} &= \frac{2}{\cosh^{-1}(2)} = 1.5186 \dots \\
 T_c^{\text{kagome}} &= \frac{4}{\ln(3 + 2\sqrt{3})} = 2.143319 \dots \\
 T_c^{\text{diced}} &= \frac{2}{\cosh^{-1} \frac{1+\sqrt{3}}{2}} = 2.405457 \dots
 \end{aligned}$$

Here, we should mention the concept of duality in lattices. The triangular lattice and the honeycomb lattice are dual to each other, as are the kagome lattice and the diced lattice. Additionally, the square lattice is self-dual. Kramers and Wannier [42, 43] demonstrated that there is a duality relation between the Ising models of these dual lattices, and they established the relationship between their transition temperatures as

follows:

$$\sinh(2J/T_c) \sinh(2J/T_c^*) = 1. \quad (6)$$

The evaluated BKT transition temperatures for the XY and six-state clock models are summarized in Table 1. For each lattice, a comparison is made with the second-order phase transition temperatures of the Ising model. The second column of Table 1 presents the coordination number for each lattice. In the case of the diced lattice, the coordination number can be either 3 or 6; however, the average value of 4 is indicated in parentheses. The third column provides the second-order phase transition temperature of the Ising model, divided by the coordination number (also in parentheses). The similarity in these values suggests that the transition temperature is approximately proportional to the coordination number.

The fourth column gives the BKT transition temperature of the XY model, divided by the transition temperature of the Ising model, with the results shown in parentheses. This value is consistently around 0.37 to 0.40, indicating the independence from the lattice structure. The two BKT transition temperatures of the six-state clock model, denoted as T_1 and T_2 , are presented in the fifth and sixth columns, respectively. Values for these temperatures, normalized by T_c of the Ising model are also included in parentheses. Again, this normalized value appears to be approximately constant, regardless of the lattice type.

5. Summary and discussion

Monte Carlo and machine learning methods were systematically employed to investigate XY models and six-state clock models on honeycomb, kagome, and diced lattices. The study examined the BKT transition temperature, in conjunction with the results of previous research focused on triangular lattices.

The Monte Carlo method was used to accurately estimate the BKT transition temperature by analyzing the ratio of correlations at different distances, which helped reduce the numerical difficulties associated with logarithmic divergence. Through FSS analysis, we identified the BKT temperature of the XY model and the two BKT temperatures of the six-state clock model. Additionally, machine learning techniques [18] extended the approach [18] by Carrasquilla and Melko [17], further validating its effectiveness in classifying low-temperature ordered, intermediate BKT, and high-temperature disordered phases by examining configurations of long-range correlations. The estimated BKT temperatures align well with those obtained from the Monte Carlo study.

In discussing the BKT transition across various 2D lattices, we have compared our results to those of the Ising model, which has known exact solutions. The BKT temperature of the XY model, along with the two BKT transition temperatures T_1 and T_2 of the six-state clock model, can be normalized by the transition temperature of the Ising model. Although the normalized values are not universal, they are nearly equal, which is a logical conclusion.

Recently, two research groups [30, 31] have reported findings on the XY model of the honeycomb lattice, and their estimates are 0.576(1)[30] and 0.560(9) [31]. The present calculation, 0.573, is consistent with both results. Some literature has pointed out a difference from Nienhuis’s exact solution [32, 33]; however, since Nienhuis’s model is also referred to as the n -vector loop model and involves different interactions. Therefore, it is expected that the numerical results from our study and the two previous papers would differ from Nienhuis’s exact result.

Research using machine learning techniques has investigated the six-state clock universality of antiferromagnetic systems with next-nearest neighbor interactions, specifically focusing on a triangular lattice [29]. In this study, the data from the ferromagnetic six-state clock model on the triangular lattice served as training data. The antiferromagnetic Ising model on the kagome lattice with next-nearest-neighbor ferromagnetic interactions has been analyzed for quite some time and represents a unique system that demonstrates six-state clock universality [50, 51]. While earlier calculations were not sufficiently quantitative, recent reports have offered new insights [52]. It will be intriguing to apply machine learning techniques to this model, especially now that we have data on the six-state ferromagnetic clock model on the kagome lattice.

We comment on the logarithmic corrections in the FSS. There are multiplicative logarithmic corrections in the amplitude of the FSS of the susceptibility [4, 7]. Accurately reproducing the theoretically predicted value of the exponent that specifies this multiplicative logarithmic correction has proven to be a challenging numerical problem [53]. It is interesting to explore whether the multiplicative logarithmic correction exponent is more straightforward to reproduce for other lattices.

The problem of the extraordinary-log surface phase transition for the three-dimensional (3D) XY model is a new topic in the XY universality [54]. The surface of 3D systems is two-dimensional, and the surface effects are classified into ordinary, special, and extraordinary transitions depending on the strength of the surface interaction. In the extraordinary transition of the XY system, it has been pointed out that the correlation function does not behave in a simple power-law manner but in a logarithmic manner. How the extraordinary-log surface phase transitions behave in surface forms of different lattices instead of cubic lattices will be the subject of future research.

Data availability statement

All data that support the findings of this study are included within the article.

Acknowledgment

The authors would like to thank Kenta Shiina, Hiroyuki Mori, and Hwee Kuan Lee for valuable discussions. This work was supported by JSPS KAKENHI Grant Number JP22K03472.

References

- [1] Berezinskii VL 1970 Destruction of Long-range Order in One-dimensional and Two-dimensional Systems having a Continuous Symmetry Group I. Classical Systems *Sov. Phys. JETP* **32** 493
- [2] Berezinskii VL 1972 Destruction of Long-range Order in One-dimensional and Two-dimensional Systems Possessing a Continuous Symmetry Group. II. Quantum Systems *Sov. Phys. JETP* **34** 610
- [3] Kosterlitz JM and Thouless D 1973 Ordering, metastability and phase transitions in two-dimensional systems *J. Phys. C: Solid State Phys.* **6** 1181
- [4] Kosterlitz JM 1974 The critical properties of the two-dimensional xy model *J. Phys. C: Solid State Phys.* **7** 1046
- [5] José JV, Kadanoff LP, Kirkpatrick S and Nelson DR 1977 Renormalization, vortices, and symmetry-breaking perturbations in the two-dimensional planar model *Phys. Rev. B* **16** 1217
- [6] Elitzur S, Pearson RB and Shigemitsu J 1979 Phase structure of discrete Abelian spin and gauge systems *Phys. Rev. D* **19** 3698
- [7] Janke W 1997 Logarithmic corrections in the two-dimensional XY model *Phys. Rev. B* **55** 3580
- [8] Landau DP and K. Binder K 2014 *A guide to MC Simulations in Statistical Physics* (Cambridge: Cambridge University Press)
- [9] Barber MN 1983 *in Phase Transitions and Critical Phenomena, vol. 8* ed C. Domb and J. Lebowitz (New York: Academic Press)
- [10] Cardy JL 1988 *Finite Size Scaling* ed J. L. Cardy (Amsterdam: North-Holland)
- [11] Binder K 1981 Finite size scaling analysis of ising model block distribution functions *Z. Phys. B* **43** 119
- [12] Hasenbusch M 2008 The Binder cumulant at the Kosterlitz-Thouless transition *J. Stat. Mech.* P08003
- [13] Tomita Y and Okabe Y 2002 Finite-size scaling of correlation ratio and generalized scheme for the probability-changing cluster algorithm *Phys. Rev. B* **66** 180401(R)
- [14] Katzgraber HG, Körner M and Young AP 2006 Universality in three-dimensional Ising spin glasses: A Monte Carlo study *Phys. Rev. B* **73** 224432
- [15] Surungan T, Masuda S, Komura Y and Okabe Y 2019 Berezinskii-Kosterlitz-Thouless transition on regular and Villain types of q -state clock models *J. Phys. A: Math. Theor.* **52** 275002
- [16] Carleo G, Cirac I, Cranmer K, Daudet L, Schuld M, Tishby N, Vogt-Maranto L and Zdeborová L 2019 Machine learning and the physical sciences *Rev. Mod. Phys.* **91** 045002
- [17] Carrasquilla J and Melko RG 2017 Machine learning phases of matter *Nat. Phys.* **13** 431
- [18] Shiina K, Mori H, Okabe Y and Lee HK 2020 Machine-Learning Studies on Spin Models *Sci. Rep.* **10** 2177
- [19] Tomita Y, Shiina K, Okabe Y and Lee HK 2020 Machine-learning study using improved correlation configuration and application to quantum Monte Carlo simulation *Phys. Rev. E* **102** 021302(R)
- [20] Kasteleyn PW and Fortuin CM 1969 Phase Transitions in Lattice Systems with Random Local Properties *J. Phys. Soc. Jpn. Suppl.* **26** 11
- [21] Fortuin CM and Kasteleyn PW 1972 On the random-cluster model: I. Introduction and relation to other models *Physica* **57** 536
- [22] Wolff U 1990 Asymptotic freedom and mass generation in the $O(3)$ nonlinear σ -model *Nucl. Phys. B* **334** 581-610
- [23] Evertz HG, Lana G and Marcu M 1993 Cluster algorithm for vertex models *Phys. Rev. Lett.* **70** 875
- [24] Hasenbusch M 2005 The two-dimensional XY model at the transition temperature: a high-precision Monte Carlo study *J. Phys. A: Math. Gen.* **38** 5869
- [25] Tomita Y and Okabe Y 2002 Probability-changing cluster algorithm for two-dimensional XY and clock models *Phys. Rev. B* **65** 184405
- [26] Vanderstraeten L, Vanhecke B, Läuchli AM and Verstraete F 2019 Approaching the Kosterlitz-

- Thouless transition for the classical XY model with tensor networks *Phys. Rev. E* **100** 062136
- [27] Li ZQ, Yang LP, Xie ZY, Tu HH, Lia HJ and Xiang T 2020 Critical properties of the two-dimensional q -state clock model *Phys. Rev. E* **101** 060105(R)
- [28] Sorokin AO 2019 Critical density of topological defects upon a continuous phase transition *Ann. Phys. (Amsterdam)* **411** 167952
- [29] Otsuka H, Shiina K and Okabe Y 2023 Comprehensive studies on the universality of BKT transitions — machine-learning study, Monte Carlo simulation, and level-spectroscopy method *J. Phys. A: Math. Theor.* **56** 235001
- [30] de Andrade F E F and DaSilva C J 2024 A study of the Berezinskii-Kosterlitz-Thouless transition in the XY model in a honeycomb lattice arXiv:2406.12076
- [31] Jiang F -J 2024 Berezinskii-Kosterlitz-Thouless transition of the two-dimensional XY model on the honeycomb lattice arXiv:2406.14812
- [32] Nienhuis B 1982 Exact Critical Point and Critical Exponents of $O(n)$ Models in Two Dimensions *Phys. Rev. Lett.* **49** 1062
- [33] Wang J, Zhang W, Hua T and Wei T-C 2021 Unsupervised learning of topological phase transitions using the Calinski-Harabaz index *Phys. Rev. Research* **3** 013074
- [34] Onsager L 1944 Crystal Statistics. I. A Two-Dimensional Model with an Order-Disorder Transition *Phys. Rev.* **65** 117
- [35] Husimi K and Syozi I 1950 The Statistics of Honeycomb and Triangular Lattice. I *Prog. Theor. Phys.* **5** 177
- [36] Syozi I 1950 Statistics of Kagome Lattice *Prog. Theor. Phys.* **6** 306
- [37] Kano K and Naya S 1953 Antiferromagnetism. The Kagome Ising Net *Prog. Theor. Phys.* **10** 158
- [38] Swendsen R H and Wang J S 1987 Nonuniversal critical dynamics in Monte Carlo simulations *Phys. Rev. Lett.* **58** 86
- [39] Wolff U 1989 Collective Monte Carlo Updating for Spin Systems *Phys. Rev. Lett.* **62** 361
- [40] Hukushima K and Nemoto K 1996 Exchange Monte Carlo Method and Application to Spin Glass Simulations *J. Phys. Soc. Japan* **65** 1604
- [41] Kingma DP and Ba J 2014 ADAM: A method for stochastic optimization arXiv:1412.6980
- [42] Kramers H A and Wannier G H 1941 Statistics of the Two-Dimensional Ferromagnet. Part I *Phys. Rev.* **60** 252
- [43] Syozi I 1972 *Phase Transitions and Critical Phenomena* vol. 1, ed C Domb and M S Green (Academic Press, London)
- [44] the present result
- [45] Olsson P 1995 Two Phase Transitions in the Fully Frustrated XY Model *Phys. Rev. Lett.* **75** 2758
- [46] Lee DH, Joannopoulos JD, Negele JW and Landau DP 1986 Symmetry Analysis and Monte Carlo Study of a Frustrated Antiferromagnetic Planar (XY) Model in Two Dimensions *Phys Rev B* **33** 450
- [47] Sun YZ, Wu Q, Yang XL, Zhou Y, Zhu LY, Chen Q and An Q 2022 Numerical Studies of Vortices and Helicity Modulus in the Two-Dimensional Generalized XY Model *Front. Phys.* **10** 851322
- [48] Weber H and Minnhagen P 1988 Monte Carlo Determination of the Critical Temperature for the Two-dimensional XY model *Phys Rev B* **37** 5986
- [49] Hsieh YD, Kao YJ and Sandvik AW 2013 Finite-size scaling method for the Berezinskii-Kosterlitz-Thouless transition *J. Stat. Mech.* P09001
- [50] Takagi T and Mekata M 1993 Magnetic ordering of ising spins on kagomé lattice with the 1st and the 2nd neighbor interactions *J. Phys. Soc. Jpn.* **62** 3943
- [51] Gia-Wei C and Oleg T 2012 Magnetic charge and ordering in kagome spin ice *Phil. Trans. R. Soc. A.* **370** 5718
- [52] Su WY, Hu F, Cheng C and Ma N 2023 Berezinskii-Kosterlitz-Thouless phase transitions in a kagome spin ice by a quantifying Monte Carlo process: Distribution of Hamming distances *Phys. Rev. B* **108** 134422
- [53] Komura Y and Okabe Y 2012 Large-Scale Monte Carlo Simulation of Two-Dimensional Classical

XY Model Using Multiple GPUs *J. Phys. Soc. Japan* **81** 113001

- [54] Hu M, Deng Y and Jian-Ping Lv JP 2021 Extraordinary-log surface phase transition in the three-dimensional XY model *Phys. Rev. Lett.* **127** 120603